Pion-proton integral cross sections at $T_\pi = 40$ to 284 MeV

B. J. Kriss,* S. Høibråten,† M. D. Holcomb,‡ M. D. Kohler,§ J. J. Kraushaar, S. Parry,‖ R. A. Ristinen, A. Saunders,¶ and W. R. Smythe
Nuclear Physics Laboratory, Department of Physics, University of Colorado, Boulder, Colorado 80309-0446

C. L. Morris, M. Rawool-Sullivan, and R. M. Whitton**
Los Alamos National Laboratory, Los Alamos, New Mexico 87545

J. T. Brack††
TRIUMF, Vancouver, British Columbia, Canada V6T 2A3

E. F. Gibson
California State University, Sacramento, California 95819

J. L. Langenbrunner‡‡
University of Minnesota, Minneapolis, Minnesota 55455
(Received 24 August 1998)

Integral cross sections for the scattering of pions by protons into angles greater than 30° (lab) have been measured at a wide range of energies spanning the delta resonance using liquid hydrogen targets. Cross sections were measured for $\pi^+ p$ scattering at 40 energies from 39.8 to 283.9 MeV and for $\pi^- p$ at 15 energies from 80.0 to 283.9 MeV. Comparisons with phase shift predictions from the Karlsruhe group show good agreement on resonance but significant deviations below 100 MeV. [S0556-2813(99)02903-9]

PACS number(s): 25.80.Dj, 25.10.+s

I. INTRODUCTION

The scattering of pions from protons is the simplest reaction mediated by the strong force that is available to experimentalists. The πp reaction determines many parameters that are of fundamental importance in low-energy interpretations of quantum chromodynamics, such as the πN coupling constant, the πN form factor, scattering lengths, and the sigma term (σ), which, through comparison with mass splittings of the baryon octet, provides a measure of chiral symmetry breaking at low energies. On the experimental level, accurate knowledge of the πp reaction is often used as an instrument calibration or normalization point for measurement of other reactions.

For more than a decade, the world's database of πN observables below 300 MeV incident pion energy has suffered from inconsistencies between various measurements of as much as six standard deviations, especially at energies below 100 MeV. These inconsistencies became apparent in 1983 with the publication of the differential cross section results of Frank *et al.* [1] at incident pion energies below 100 MeV. These new data disagreed with previous measurements of Bertin *et al.* [2], and phase shift analyses [3,4] showed that the results of Frank *et al.* also disagreed with the total cross sections of Bussey *et al.* [5] near 90 MeV. Since then, several groups have attempted to resolve the discrepancies [6–12]. In general the newer results, consisting mainly of differential cross sections, have tended to agree with the pre-meson-factory results near the 3-3 (delta) resonance but show a consistent difference with the older results at energies below the resonance.

In 1989, a new experimental observable for πp elastic scattering — the partial total, or integral, cross section — was measured by Friedman *et al.* [13]. The technique involves inferring the integral of the differential cross section outside some forward angle by measuring the beam intensity transmitted into that cone. By comparing the transmitted and incident beam intensities, the integral cross section is determined.

High accuracy is not easily achieved in experiments of this type. The fraction of the beam removed by elastic scattering in the hydrogen target is less than a third of a percent at the lowest energies reported here and only a few percent

*Present address: Lockheed Martin Mission Systems, 9970 Federal Drive M/S 01B, Colorado Springs, CO 80921.
†Present address: FFIVM, N-2007 Kjeller, Norway.
‡Present address: Johnson Matthey Semiconductor Packages, Chippewa Falls, WI 54729.
§Present address: Bridgewater State College, Department of Physics, Bridgewater, MA 02324.
‖Present address: Department of Fish and Game, Region III, 333 Raspberry Rd., Anchorage, AK 99518.
¶Present address: Los Alamos National Laboratory, Los Alamos, NM 87545.
**Present address: Florida State University, P.O. Box 4390, Tallahassee, FL 32306-4390.
††Present address: University of Colorado, Boulder, CO 80309-0446.
‡‡Present address: Bechtel Nevada, P.O. Box 809, Los Alamos, NM 87544.

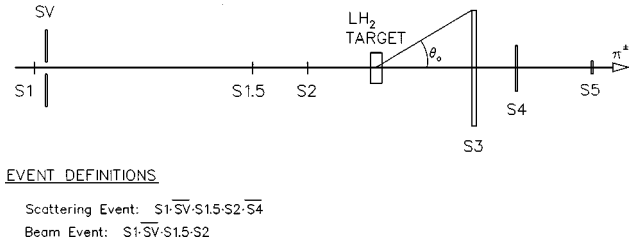

FIG. 1. Diagram of the experimental setup. All counters are plastic scintillators. The logic conditions for the experiment are shown. The figure is not drawn to scale.

on resonance. To measure the beam removal fraction at low energies to within a few percent thus requires counting accuracy in the fifth digit, including electronic stability and all corrections such as for pion decay. On the other hand, the uncertainties for integral cross section measurements are not dominated by the statistics of the scattered particles, as in differential cross section measurements. For the integral cross section measurements, the dominating uncertainties are systematic.

Friedman *et al.* used solid CH_2 targets, and subtracted the background from solid carbon targets in an experiment that scaled counts in scintillators. Data were not recorded directly to tape for off-line analysis. Solid targets have the advantage of simplicity in differential cross section experiments where the scattering kinematics is fully defined, allowing elimination of the carbon background. In beam attenuation measurements with undefined kinematics, however, that advantage is lessened by the carbon elastic and inelastic backgrounds.

This paper reports an experiment which incorporated several technical changes in the measurement of the integral cross section. The experiment was performed at the Clinton P. Anderson Meson Physics Facility (LAMPF) in Los Alamos, New Mexico. The experiment used liquid hydrogen targets which yielded a target-full–to–target-empty ratio of scattering events of about 3 at the lower energies and about 10 on resonance. A complete data acquisition system was used, and time-of-flight and pulse-height information for all scattering events were recorded on tape for off-line analysis.

II. EXPERIMENTAL APPARATUS

The experiment was conducted using the P^3W pion channel at LAMPF [14]. The experiment employed the transmission method [15] to measure integral cross sections. A diagram of the experimental setup is shown in Fig. 1. The scintillator dimensions are listed in Table I.

Four plastic scintillators (S1, SV, S1.5, and S2) defined the beam. The two smaller scintillators S1 and S2 defined the beam spot on the target. S1.5 was mounted with the light guide rotated 180° to the opposite side of the beam line from the S2 light guide. This eliminated the possibility of coincidences being registered by Čerenkov light produced by beam particles passing though the light guides. The annular veto counter, SV, removed events from all LAMPF beam micropulses having extra pions outside the trajectories defined by S1 and S2. This greatly reduced the effect of beam doubles and higher-order multiples on the cross sections. All beam particles were counted according to a coincidence definition between S1, S1.5, S2 and an anticoincidence with SV, or $\mathrm{BEAM}=(\mathrm{S1}\times\overline{\mathrm{SV}}\times\mathrm{S1.5}\times\mathrm{S2})$.

Downstream of the target, a movable detector S3 subtended a cone of either 30° or 20° half-angle as seen from the target center (θ_0 in Fig. 1), and defined the experimental solid angle. The S4 counter defined the solid angle for events recorded to tape for off-line analysis. This solid angle was much smaller than that of S3. These events were defined as a coincidence between BEAM and an anticoincidence with the S4 counter or $\mathrm{BEAM}\times\overline{\mathrm{S4}}$. In addition, S4 continuously monitored the efficiency of S3 and the associated electronics for counting beam pions, calculated as

$$\eta=\frac{\mathrm{BEAM}\times\mathrm{S3}\times\mathrm{S4}}{\mathrm{BEAM}\times\mathrm{S4}}.$$

The value of η was stable between 0.9999 and 1.0000.

Another scintillator S5 was placed downstream from the target, providing a 6.2 m flight path between S1 and S5. When collecting data at energies where there was significant electron contamination of the pion beam exiting the channel, the difference between pion and electron time of flight (TOF) from S1 to S5 was used to provide a verification of the energy calibration for every data run. In addition, the TOF separation of pions, muons, and electrons over this distance was used to monitor the pion fraction of the incident beam at the center of the target.

Typical beam rates varied from 500 to 2500 particles per second. The full momentum spread of the beam was 1–1.3 % at the lowest energies (40 and 55 MeV) and was typically 0.3–0.5 % at all other energies.

TABLE I. Dimensions of the seven plastic scintillator counters used in the experiment, and their locations relative to the target. All the counters were circular except S1.5 and S5, which were square. In the diameter column, the full edge length of the two square scintillators is listed. All dimensions are in centimeters.

Counter	Inner diameter	Outer diameter	Thickness	Distance from target
S1		1.5	0.159	-142.9
SV	1.5	20.0	0.318	-140.7
S1.5		2.9	0.159	-19.4
S2		1.5	0.159	-11.6
S3		30.0	1.270	26.0
S4		12.0	0.318	58.2
S5		10.2	0.635	479

III. TARGET

The two liquid hydrogen (LH_2) targets were vertical cylinders, 3.5 cm diameter by 7.6 cm high and 6.0 cm diameter by 10.2 cm high, contained in an aluminum vacuum chamber with Mylar entrance and exit windows. The targets could be drained to provide empty targets for background measurements. Each target had its own set of entrance and exit windows in the vacuum chamber. An electric motor drove two jacks that could raise or lower the vacuum chamber, providing a way to bring either target into the beam line. The vertical cylindrical target cells were made from 125-μm-thick Mylar wrapped around stainless steel end caps. For insulation against radiant heat transfer, both targets were wrapped with ten layers of 6 μm aluminized Mylar. The S2 counter was placed as near as possible (about 11 cm) to the entrance windows in the vacuum chamber. The entrance windows were made from 125-μm-thick Mylar and were 5.1 cm in diameter. The Mylar exit windows were 250 μm thick and 19.1 cm in diameter. The exit windows subtended a cone of approximately 49° half-angle as seen from the target center, easily allowing all pions that scattered into the solid angle defined by S3 to pass through the window.

The computation of the number of protons/cm^2 in the targets was complicated by the fact that the beam axis was perpendicular to the axis of symmetry for the cylindrical cells. A parallel beam incident on a vertical cylindrical target will see an average path length through the target smaller than the diameter of the cell. The effective thicknesses of the target cells were measured by a stack of nine circular scintillators, ST1–ST9, forming a range spectrometer in a manner similar to that of Frank *et al.* [1]. All scintillators were 5.1 cm in diameter except ST1 which was smaller to match the beam defining counters; it defined the acceptance of the range spectrometer. ST3–ST6 were 1.69 mm thick; all others were 3.39 mm thick. Two distances from the target center to ST1 (53 cm and 69 cm) were used. The target thickness was measured by determining the difference in total thickness of aluminum absorbers necessary to adjust the pion beam energy so as to stop the pions at the same depth in the stack under target full and target empty conditions.

For these thickness measurements, data were taken with a π^+ beam of 51.1 MeV incident energy. The data were analyzed off line, where pulse height [analog-to-digital converter (ADC)] and time-of-flight [time-to-digital converter (TDC)] information from ST1–ST9 and the beam defining scintillators ensured that electrons and muons in the beam were eliminated. The average stopping position in the stack was determined from the distribution of number of stops in each scintillator. For the 6 cm LH_2 target, the equivalent thickness of aluminum was found to be 1.088 ± 0.025 g/cm^2. The target thickness was then calculated to be 0.422 ± 0.010 g/cm^2 using the known ratio (2.582) of pion energy losses [16] in Al and in LH_2. Dividing by the density of LH_2 at the target temperature of 20.4 K (0.0708 g/cm^3) gives a target thickness of 5.95 ± 0.14 cm, slightly less than the diameter of the target, as expected. The same technique was employed to determine the thickness of the 3.5 cm target, with similar results.

The uncertainty in the final target thickness takes into account a 0.5% uncertainty in the ratio of energy losses in the two materials. In addition, inexact knowledge of the ratio of ortho- to para-hydrogen introduced an uncertainty of 0.2%, and temperature variations in the target contributed another 1% to the target thickness uncertainty.

The range spectrometer measurement of target thickness was repeated. Combining the results in a weighted average resulted in a final value of 0.4208 ± 0.0082 g/cm^2 for the 6 cm target. This thickness was used in calculating the final cross sections.

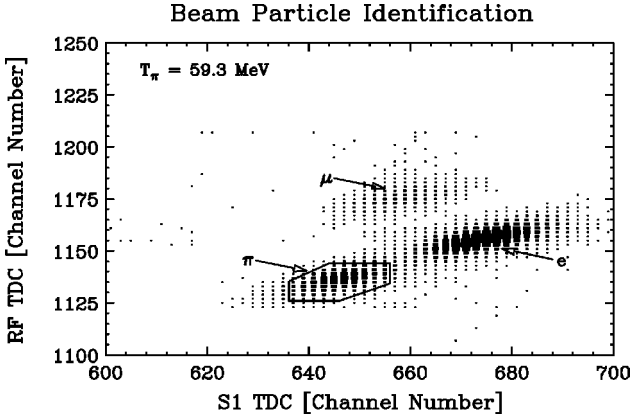

FIG. 2. Sample TOF histogram at a π^+ energy of 59.3 MeV showing beam particle identification. The horizontal axis is the time difference between S1 and S2; the vertical axis is the particle flight time (*modulo* the accelerator rf period) through the P^{3}W channel to S2, referenced to the accelerator rf signal. The time calibration of the TDC for this figure is 50 ps per channel. The polygon identifies beam pions used in the data analysis.

IV. DATA ANALYSIS

ADC and TDC information taped during the experiment were analyzed off line to extract the yields and perform systematic checks. Figure 2 shows a typical beam event histogram used for incident particle identification. The histogram illustrates the polygon TOF cut used to separate pion beam events from those produced by muons and electrons. In addition to the TOF cut, pulse-height cuts were placed on the S1, S1.5, and S2 ADC data words. The upper-level pulse height cut on S1 eliminated all beam events from doubles and higher-order multiples that missed SV but were part of the S1 and S2 trajectories. The pulse-height cuts on the S1.5 and S2 ADC data words removed pulses of large amplitude from both scintillators. This rejected events in which the incident pion underwent a hadronic reaction in either detector and deposited a significant amount of energy.

The S5 TDC spectrum was used to verify the beam pion identification, as discussed earlier, and shown in Fig. 3. For most of the experiment, S1 and S5 were separated by approximately 6.2 m. The upper and lower histograms display data from the same run, but only particles that have passed the TOF and pulse height cuts for pion identification such as shown in Fig. 2 are included in the lower plot. The data in Fig. 3 were taken at 110 MeV incident pion energy. The length of the P^{3}W channel is such that pions at this energy, and at several others used in this experiment, arrive at S2 at nearly the same time as electrons or muons from subsequent

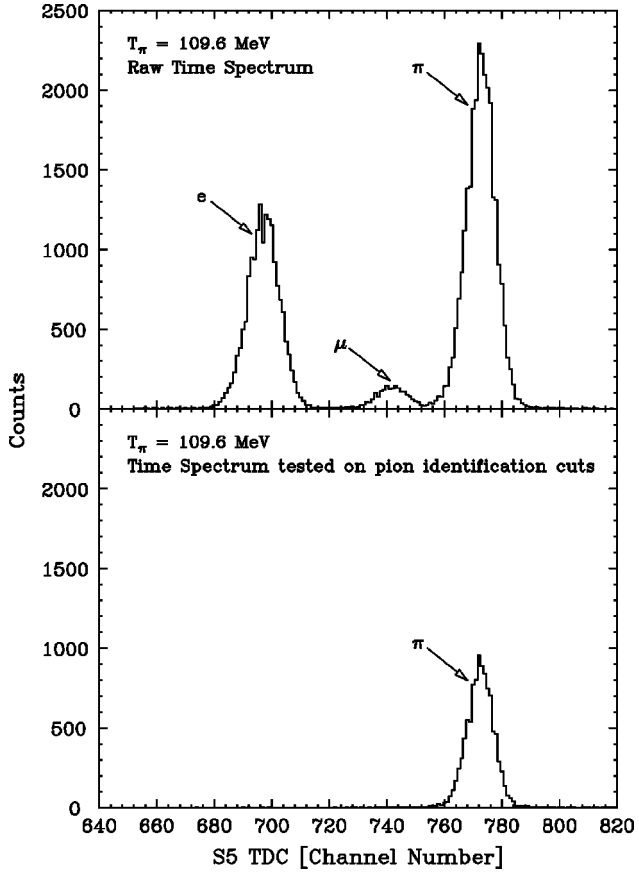

FIG. 3. S5 TOF spectra used to verify beam particle identification. Sample TOF histograms are shown for π^+ data at an incident energy of 109.6 MeV. The horizontal axis on both histograms is the time difference between S1 and S5 in units of TDC channel number. The time calibration of the TDC for this figure is 60 ps/channel. A raw time spectrum, shown in the upper histogram, displays the separation between the three particle groups that exit the P^3W channel. The time spectrum in the lower histogram is tested on the TOF and pulse height cuts.

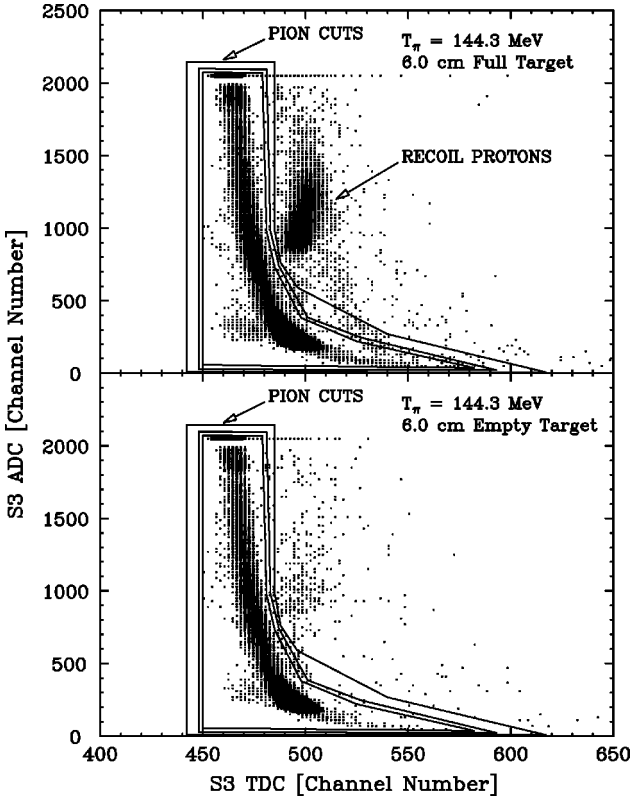

FIG. 4. Recoil proton identification in the transmission counter. Sample histograms from a pair of full and empty data runs at a π^+ energy of 144.3 MeV. On both histograms, the vertical axis is the S3 pulse height spectrum in units of ADC channel number, and the horizontal axis is the time difference between S1 and S3 in units of TDC channel number. The time calibration of the TDC is 60 ps per channel. Polygon cuts of this type were used to remove pions that scattered into S3 from the integral cross sections without removing recoil protons from the target that scattered into S3. The variation in the three polygons shown illustrates the technique used to examine the sensitivity of the cross sections to the exact definition of the pion identification polygon.

rf cycles, requiring cuts much tighter than the example shown in Fig. 2. At these energies, a large fraction of the beam pions were eliminated by these very tight cuts, resulting in fewer pions in the lower histogram of Fig. 3. Such a reduction in the number of effective beam pions is not a disadvantage in a transmission experiment of this type, since statistical errors do not dominate the final uncertainties. Ensuring a pure pion beam, however, is crucial.

Scattering events containing pions that scattered into the solid angle defined by S3 are not part of the integral cross section and must be removed by the analysis process. Figure 4 shows typical histograms used to remove these pions. The histograms show π^+ data from a pair of full and empty runs in the 30° geometry at an incident energy of 144.3 MeV. Both histograms show the S3 pulse height spectrum plotted versus the particle TOF between S1 and S3. The upper histogram displays the polygon cuts used to separate those events in which the pion scattered into S3 from those events in which the recoil proton from the full target scattered into S3. Pions inside the polygons are the sole contributors to the number of pions that scattered into S3. The pion distribution includes pulses of large amplitude due to pion absorption in S3. These pion events are shifted to apparent shorter flight times by discriminator walk. The protons outside the polygons are ejected from the LH_2 target by backscattered pions that are part of the integral cross section. In the lower histogram, the proton distribution is largely missing because the histogram is from an empty target run. Like all the other cuts applied in the analysis, the same polygon cuts were applied on these S3 histograms for corresponding full and empty runs.

TOF information was used along with the 2280 cm flight path from the production target to S1 to determine the incident beam energy. The flight path consisted of the measured 1875.3 cm channel length [14] and the distance from the channel exit to S1. This TOF information was available from the event data for each run. For center-of-target energies from 39.8 to 119.4 MeV, the TOF difference between pions and electrons from the production target to S1 was used. From 119.4 to 283.9 MeV, the TOF difference for pions and protons was used. The energy losses in all materials along the beam path were included in this analysis. These data provided a $\pm 0.5\%$ uncertainty in the energies. The calibra-

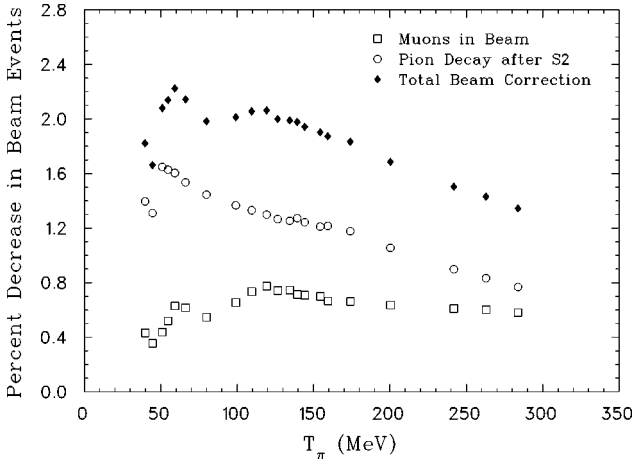

FIG. 5. Monte Carlo beam corrections. Sample π^+ beam corrections generated from the Monte Carlo program. The corrections indicate the decrease in beam coincidences due to contamination by muons from pion decay. The statistical uncertainty in most of these corrections is less than 0.02% of the cross section, which is too small to be seen on the scale of the plot.

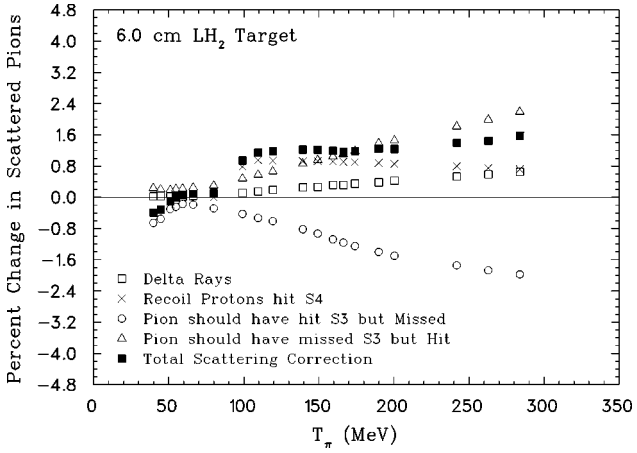

FIG. 6. Monte Carlo scattering corrections. Sample $\pi^+30°$ scattering corrections generated from the Monte Carlo program. These corrections are for the 6.0 cm LH_2 target only. The corrections account for four different processes (described in the text) that affect the scattered pion count. The statistical uncertainties are too small to be seen on the scale of the plot.

tion was verified by S1 to S5 TOF at energies below 160 MeV with $\pm 1.0\%$ accuracy and at energies between 160 and 250 MeV with accuracy decreasing to $\pm 5\%$.

The Monte Carlo program GEANT [17] was used to account for the effects of pion decay, multiple Coulomb scattering, and other physical processes that artificially increase or decrease the number of beam and scattered pions. Figure 5 shows two Monte Carlo–generated corrections to the beam for decay of pions downstream from the last bending magnet in the channel. One of these two corrections is for pion decay upstream of S2; the other is for pion decay after S2. The resulting muons form beam coincidences that cannot be distinguished from pions via the polygon cut presented in Fig. 2 because of the small TOF difference between the two particles. A second correction was made for pion decay between S2 and the center of the target.

Four Monte Carlo–generated corrections for scattered particles are shown in Fig. 6. The delta-ray correction deals with knockout atomic electrons from the target that can hit S3 and appear to be pions in the S3 polygon cut. The proton correction accounts for the fact that backscattered pions can produce recoil protons in the target that travel through both S3 and S4. These events should be part of the integral cross section but they are removed from acquisition because the signal in S4 vetoes the scattering event trigger logic as shown in Fig. 1. This correction is dependent on the incident pion energy and the S4 solid angle (see Sec. V).

The remaining two corrections in Fig. 6 are for the effective solid angle, and deal with processes such as multiple scattering and decay, which allow events in which pions scattered outside the solid angle defined by the transmission counter to be vetoed by a hit in S3 or allow events in which pions scattered inside the defined solid angle to be added to the scattered events by not producing a hit in S3. These two corrections tend to cancel each other.

A correction, not shown in the Monte Carlo correction figures, was made to the cross sections for the difference between full and empty target loss of muons from pion decay. Some low-energy muons from pion decay, those traveling backward in the pion center of mass frame, stop in the full target but not the empty target, thus artificially increasing the cross section. This occurs only for the lowest three incident pion energies, and the correction was about 8% of the cross section at 40 MeV, 4% at 45 MeV, and 1% at 51 MeV.

V. SYSTEMATIC CHECKS

A number of tests were performed to assess the systematic uncertainties associated with various components of the experiment. These were related to the beam energy and composition, the geometry of the experimental setup, and the data analysis.

As mentioned above, the energy of the beam was determined for each run by TOF techniques over multiple flight paths, providing redundant results. In addition, beam rate tests were performed in which the beam coincidence rate varied from 100 to 3000 particles per second, and the size and location of the beam defining counters were varied. The diameter of S1 and S2 and the hole in SV were decreased from 1.3 to 1.0 cm, and S1 and SV were moved about 30 cm closer to the target. No significant effects on the cross sections were seen with these tests. Near 67 MeV, one other test concerning the beam energy was performed, in which the incident pion energy was adjusted for full and empty target runs to match the center-of-target energies. This required separate Monte Carlo simulations for the two beam energies. A 0.5% difference was observed in the cross sections, well within the uncertainties.

The solid angle subtended at the target by the S4 detector determined the rate at which forward recoil protons vetoed good events at energies where these protons had sufficient energy to pass through S3 and hit S4. The Monte Carlo–generated correction to the cross sections for this effect was tested by changing the distance from the target to S4 at selected energies. Data were taken at 174.1 MeV with the S4

detector moved 30 cm upstream from the nominal position. This movement of S4 nearly quadrupled the proton correction, yet the corrected cross sections agreed within errors. Similar tests were performed at 99.2 MeV and 262.9 MeV, with similar results.

In software, pulse height and TOF cuts were placed on a two-dimensional histogram of S3 ADC vs TDC to separate forward scattered pions from recoil protons, as shown in Fig. 4. The size and placement of these cuts were varied as shown to test the effect on the resulting cross sections. The three polygons shown in the figure gave cross sections differing by a maximum of 0.2%. This degree of stability in the extraction of the yields was found at all energies.

An independent method for removing the protons from the forward scattered pions is to insert an absorber upstream of the S3 counter. This was done as a check on the software cuts, using an 8-mm-thick copper absorber of the same diameter as the S3 counter. This absorber was less than 100% efficient since a hole 10 cm in diameter was cut in it to allow the beam to pass through, but this region represents a negligible fraction of the proton solid angle compared to that of the absorber. The resulting cross sections, including those from the variations in the software cuts, agreed within the stated uncertainties with those from the nominal setup.

In addition to the systematic checks described above, a limited data set (eight energies for π^+, one energy for π^-) was taken with the S3 counter positioned so that it defined a forward cone of 20° half angle. The cross sections were extracted as for the 30° data, and compared to phase shift calculations. These results were consistent with those obtained at 30° and are not included in this paper.

VI. RESULTS

The integral cross sections listed in Table II were calculated using the expression

$$\sigma_{\rm int}=\frac{A}{N_A T}\ln\left(\frac{R_0}{R}\right).$$

Here A is the atomic mass of hydrogen, N_A is Avogadro's number, T is the target thickness in g/cm^2, and R and R_0 are the fractions of incident pions reaching the S3 counter for full and empty targets, respectively, subject to the cuts and corrections discussed in Sec. IV. The uncertainties shown in Table II include all statistical and systematic uncertainties added in quadrature, except the $\pm 0.5\%$ uncertainty in the energy calibration.

Scattering data for $\pi^- p$ were not taken at all the incident pion energies. There is the consideration that these data may not be as useful as the $\pi^+ p$ data due to the inclusion of the charge exchange (CEX) reaction in the $\pi^- p$ data. In principle, a simple subtraction of the known CEX cross sections could yield the $\pi^- p$ elastic partial total cross section. But the CEX cross sections form a large part of the quantity measured here and the large uncertainties in the existing CEX data would give uselessly large uncertainties in the resulting cross sections. For example, near 100 MeV the CEX cross section makes up approximately 80 ± 4 % of the integral $\pi^- p$ cross section outside of 30°. If the CEX is subtracted from the partial total to extract the elastic contribution, an uncertainty of about 40% is obtained.

TABLE II. The π^+ 30° and π^- 30° integral cross sections. The uncertainties shown include statistical and systematic contributions. The $\pm 0.5\%$ uncertainty in the beam energy has not been included.

T_π (MeV)	π^+ 30° (mb)	π^- 30° (mb)
39.8	8.5±0.7	—
40.5	8.3±1.5	—
44.7	9.2±0.8	—
45.3	9.4±0.7	—
51.1	12.8±0.7	—
51.7	11.8±0.8	—
54.8	13.2±0.5	—
59.3	15.8±0.4	—
66.3	20.4±0.4	—
66.8	21.0±3.2	—
80.0	29.7±0.7	14.6±0.6
89.3	39.1±2.0	—
99.2	52.9±0.7	23.4±1.1
109.6	69.1±1.0	—
119.4	87.6±1.4	34.6±1.1
125.1	102.8±1.8	—
126.6	103.3±1.6	—
134.5	117.7±2.6	—
139.4	128.9±2.2	50.4±1.4
144.3	139.9±2.9	—
149.3	153.7±2.0	57.0±1.3
154.4	159.3±3.3	—
159.4	165.8±3.7	61.1±1.4
166.4	166.1±2.2	—
169.5	173.3±3.5	67.2±1.6
174.1	169.5±1.9	66.9±2.0
174.5	167.9±9.8	—
179.7	163.3±1.6	65.2±1.2
184.7	162.0±3.4	—
189.9	155.3±2.1	61.2±1.6
195.2	149.8±3.1	—
200.4	141.4±2.1	58.2±1.3
205.5	130.9±3.0	—
210.7	127.2±1.8	—
221.1	109.2±1.9	48.5±1.1
231.4	99.8±1.8	—
241.9	85.8±1.5	37.5±0.9
252.3	74.9±1.3	—
262.9	65.6±0.7	32.8±0.8
283.9	52.6±1.2	27.3±0.7

VII. COMPARISONS AND DISCUSSION

The $\pi^+ p$ integral cross sections are shown in Fig. 7 as ratios to the the VPI phase shift prediction of Arndt *et al.*, SM95 [4]. Also shown are the previous measurements of Friedman *et al.* [13] and the Karlsruhe solution KA84 [3]. The two experiments are in good agreement throughout most of the energy range, with only the very lowest- and highest-

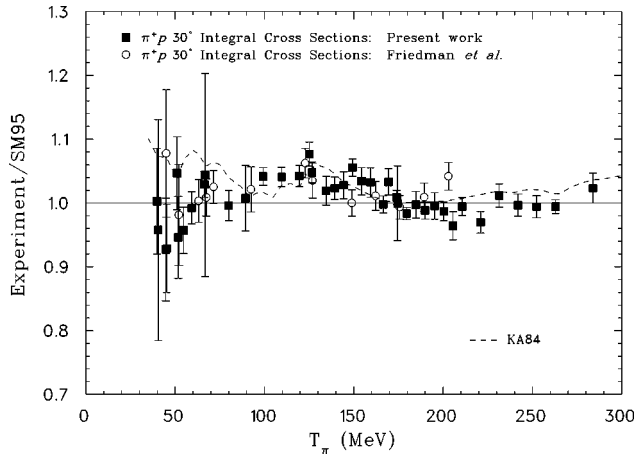

FIG. 7. Ratios of the π^+ 30° integral cross sections from the present work and from Ref. [13] to the SM95 predictions. The KA84 solution is also shown as a ratio to SM95.

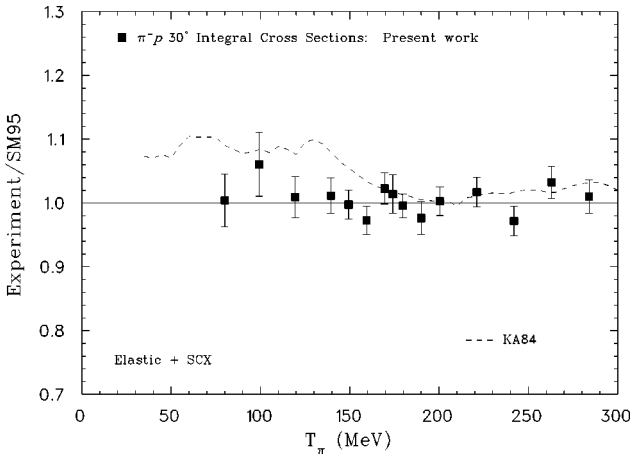

FIG. 8. Ratios of the π^- 30° integral cross sections from the present work to the VPI SM95 predictions. The Karlsruhe solution KA84 is also shown as a ratio to SM95.

energy points of Friedman *et al.* differing by as much as a standard deviation from the present measurement. The data are described best by the SM95 phase shift solution, especially in the region below 100 MeV. This is no surprise, since this solution is based on more recent databases, to which KA84 did not have access.

Thus the present measurements tend to support the more modern database, including the low-energy differential cross sections. While the general trend toward lower cross sections at energies below 100 MeV appears correct, there are suggestions [18] that the present results and those of Friedman *et al.* [13] may be higher than the integral from 30° to 180° of recently measured differential cross sections [1,6,7] at similar energies. The reasons for these apparent differences are not understood.

While SM95 provides the better fit to the full data set, it falls about one standard deviation lower than the present data in the region between 100 and 170 MeV. It has been shown that SM95 provides a good fit to recent differential cross section data in this region [11].

The π^-p results are compared with KA84 and SM95 in Fig. 8. As with the π^+p data, the trend is toward agreement with both phase shift solutions near resonance, but with the data dropping below the KA84 solution at lower energies. This is in agreement with the SM95 phase shift prediction. It should be pointed out that the curves representing the phase shift analyses in the figures contain contributions from the elastic channel outside of 30° and also from the total charge exchange reaction, while the data points do not include some small fraction of the charge exchange reaction inside 30°. This is due to the nonzero efficiency of scintillators for detection of the neutral reaction products of the charge exchange reaction, which would veto some CEX events inside the 30° cone as described above. While this effect is small, it may account for as much as 0.01–0.02 of the observed differences in the ratios shown in Fig. 8.

In conclusion, these new data add to the modern database for πN scattering at low incident pion energies, and reinforce earlier findings that pre-meson-factory phase shift analyses suffer from deficiencies in the database of that time period.

ACKNOWLEDGMENTS

The authors thank the LAMPF staff for assistance in the design, construction, setup, and running of this experiment. This work has been funded in part by the U.S. Department of Energy.

[1] J. S. Frank *et al.*, Phys. Rev. D **28**, 1569 (1983).
[2] P. Y. Bertin *et al.*, Nucl. Phys. **B106**, 341 (1976).
[3] KH80 and KA84 PSA solutions of the Karlsruhe-Helsinki Group, R. Koch and E. Pietarinen, Nucl. Phys. **A336**, 331 (1980); R. Koch, *ibid.* **A448**, 707 (1986).
[4] R. A. Arndt, R. L. Workman, and M. M. Pavan, Phys. Rev. C **49**, 2729 (1994); R. A. Arndt, I. I. Strakovsky, R. L. Workman, and M. M. Pavan, *ibid.* **52**, 2120 (1995).
[5] P. J. Bussey *et al.*, Nucl. Phys. **B58**, 363 (1973).
[6] J. T. Brack *et al.*, Phys. Rev. C **34**, 1771 (1986); J. T. Brack *et al.*, *ibid.* **38**, 2427 (1988); J. T. Brack *et al.*, *ibid.* **41**, 2202 (1990); J. T. Brack *et al.*, *ibid.* **51**, 929 (1995).
[7] C. Joram *et al.*, Phys. Rev. C **51**, 2159 (1995).
[8] R. Wieser *et al.*, Phys. Rev. C **54**, 1930 (1996).
[9] U. Wiedner *et al.*, Phys. Rev. D **40**, 3568 (1989).
[10] M. E. Sevior *et al.*, Phys. Rev. C **40**, 2780 (1989).
[11] M. M. Pavan, πN Newsletter No. 11, Proceedings of the 6th International Symposium on Meson-Nucleon Physics and the Structure of the Nucleon, 1995, Vol. II, p. 117, Report No. ISSN 0942-4148; M. M. Pavan, Ph.D. thesis, University of British Columbia, 1995.
[12] G. J. Hofman *et al.*, Phys. Rev. C **58**, 3484 (1998).
[13] E. Friedman *et al.*, Phys. Lett. B **231**, 39 (1989); E. Friedman *et al.*, Nucl. Phys. **A514**, 601 (1990); E. Friedman *et al.*, Phys. Lett. B **254**, 40 (1991).
[14] ''LAMPF User's Handbook,'' Report No. MP-DO-3-UHB,

Los Alamos National Laboratory, 1984.
[15] G. Giacomelli, *Progress in Nuclear Physics* (Pergamon Press, Oxford, 1970), Vol. 12, Pt. 2.
[16] S. M. Seltzer and M. J. Berger, U.S. Department of Commerce, National Institute of Standards and Technology (private communication).
[17] GEANT, version 3.16, high energy physics detector description and physical process Monte Carlo simulation program, Applications and Software Group, Computing and Networks Division, CERN, Geneva, Switzerland, 1993.
[18] R. A. Ristinen *et al.*, πN Newsletter No. 11 [11], p. 1.